Flow Characteristics in a 3D-Printed Rough Fracture

Article *in* Rock Mechanics and Rock Engineering · July 2022

DOI: 10.1007/s00603-022-02854-3

3 authors, including:

Ye Jianhong
Chinese Academy of Sciences
61 PUBLICATIONS **1,300** CITATIONS

SEE PROFILE

Rock Mechanics and Rock Engineering
https://doi.org/10.1007/s00603-022-02854-3

ORIGINAL PAPER

Flow Characteristics in a 3D-Printed Rough Fracture

Yan Zhang[1] · **Jianhong Ye**[2] · **Peixin Li**[1,2]

Received: 1 July 2021 / Accepted: 12 March 2022

Abstract
Based on the 3D-printing technique, totally 44 transparent specimens each containing a single fracture with 4 types of aperture and 11 types of roughness are designed and printed in this study. To perform the seepage test for these printed single fractures, an apparatus is designed and successfully manufactured to measure the water flux and the hydraulic gradient of seepage. Using the designed equipment, a series of seepage tests are conducted for the 44 3D-printed specimens. It is confirmed by the test results that the flow speed of seepage and the hydraulic gradient can always be mathematically described by the Forchheimer equation ($I = A\mathrm{u} + B\mathrm{u}^2$), regardless of the aperture and the roughness of fractures; and that the linear drag coefficient A and the nonlinear drag coefficient B in the Forchheimer equation are significantly affected by the aperture and roughness of fractures. As for the smooth fracture, the traditional cubic law is merely applicable to the situation in which the hydraulic gradient $I < 0.01$. Based on these experimental results, a new set of formulations illustrating the relationship between the linear drag coefficient A, the nonlinear drag coefficient B and the aperture e, the roughness JRC of fractures is firstly established in this study. Finally, adopting the method of solving the Navier–Stokes equation, the seepage process in single rough fractures is numerically investigated. The comparative analysis shows that the numerical result agrees quite well with the experimental results. Most importantly, the numerical results can clearly reveal that there are typical boundary layers close to the two walls of fractures in the process of seeping; and the velocity and pressure fields in fractures also can be observed intuitively from the numerical results. Summarily, it is recognized that the numerical method is a reliable and feasible method to study the seepage in fractures, and is a beneficial complement to the laboratory tests.

Highlights

- Flow characteristics of water in single rough fracture with large aperture is explored through experimental and numerical method.
- Two neat formulations are proposed to characterize the relationship between the linear and nonlinear drag coefficient in Forchheimer equation and the JRC, aperture e for the seepage flow in fractures.
- It is validated that the solving of the Navier-Stokes equation incorporating turbulent models can reliably simulate the flow characteristics of water in fractures.

Keywords Seepage flow in fractures · Single rough fracture · 3D-printing technique · Drag coefficient · Forchheimer equation · Navier–Stokes equation

1 Introduction

The fractures in the jointed rock mass are the main channels to transport water and other liquid materials. In recent years, the research on the seepage in fractures has been paid more and more attention, mainly because the seepage in fractures has brought significant risks to underground excavation projects, such as mineral mining and traffic tunnel excavation. For instance, water bursting accidents occur every year in

✉ Jianhong Ye
yejianhongcas@gmail.com

[1] School of Safety Science and Emergence Management, Wuhan University of Technology, Wuhan 430070, China

[2] State Key Laboratory of Geomechanics and Geotechnical Engineering, Institute of Rock and Soil Mechanics, Chinese Academy of Sciences, Wuhan 430071, China

Published online: 22 April 2022

China, causing many casualties. Therefore, it is of great significance to study the seepage characteristics in rock fractures for analyzing the seepage field in fractured rock mass, and for guiding to quantitatively evaluate the risk of water bursting and water gushing in the design of underground rock engineering.

Single fracture is the basic component of a complex fracture network. Since a real fracture network is too complicated to be analyzed, many scholars have conducted many systematic and productive works on the seepage characteristics in a single fracture. For example, Lomize (1951) and Louis (1974) proved the validity of the cubic law for laminar flow through the laboratory tests of water flow in a horizontal single fracture. Through laboratory tests, Patir and Cheng (1978) found that the seepage in fracture with a smooth surface was significantly different from that with a rough surface, and it was indicated that the roughness intensively affects the seepage of water in fractures. Based on plenty of test data, Barton et al. (1985) proposed a JRC correction method, which combined the equivalent hydraulic aperture with the hydraulic aperture together, and suggested that an equivalent hydraulic aperture should be used in the cubic law. Amdei and Illangasekare (1994), Su et al. (1995) proposed a modified cubic law based on the seepage test adopting simulated natural fractures.

Wang and Su (2002) proposed a method to characterize the aperture and surface roughness of fractures and then established the relationship between the seepage characteristics in single fractures and the equivalent hydraulic aperture. Xu et al. (2003) proposed that the Hypercubic law and sub-cubic law could be used to describe the seepage characteristics in rough fractures based on a series of seepage tests for fractures. He et al. (2010) prepared ten cylindrical cement samples for seepage test, each sample contained a single fracture with different JRC values. Their test results indicated that JRC has a significant influence on the seepage in a single fracture under the low confining stress condition. However, the influence of JRC tends to be less under the condition of high confining stress. Some valuable works have also been carried out for the nonlinear seepage in fractured rock mass in the past 30 years. For example, Zimmerman and Bodvarsson (1996) theoretically derived that the applicable condition for cubic law for single fractures was that the Reynolds number $\mathrm{Re} << 1$. Whereafter, through the seepage test for the single fracture in natural sandstone, Zimmerman et al. (2004) found that there was a weak inertial effect for the seeping water when Re was in the range of 1–10, resulting in that the flow speed and hydraulic gradient will no longer maintain a linear relationship. Zhang and Nemcik (2013) carried out a series of seepage tests for the single fracture in natural sandstone formed by adopting the Brazilian splitting test. Their results indicated that fluid could also present prominent nonlinear seeping characteristics even at a very small flowing speed.

Due to the limitation of the means of making rock fractures in laboratory, previous researchers could only make the imitating natural rock fractures by the way of cylinder splitting (Tian et al. 2021; Chen et al. 2015; Liu et al. 2020). The fractures produced were all tensile fractures, and their apertures generally were tiny (on the magnitude of several hundred microns). The cylinder splitting method basically cannot produce the fractures with an aperture more significant than 1 mm, and it also cannot control the roughness coefficient JRC and the aperture of fractures. With the rise and progress of 3D-printing techniques, it is possible to produce complex fractures with desired aperture and roughness. 3D-printing technique can accurately design and control the roughness coefficient JRC and the aperture of fractures. It has become a popular auxiliary tool to study the seepage in fractures in recent years (Ni et al. 2018; Tan and Wang 2020; Phillips et al. 2020; Zhao et al. 2017; Wang et al. 2019). A series of typical seepage tests have been carried out in the recent decade to study the seepage characteristics of fractures under different roughness and aperture. In these works, some only established the relationship between the linear coefficient A, as well as the nonlinear coefficient B in the Forchheimer Equation ($I = \mathrm{A}u + \mathrm{B}u^2$) and the aperture e (Chen et al. 2015), but not consider the influence of JRC. Furthermore, some works did not establish the relationship among A, B, JRC, and the aperture e at all (Tian et al. 2021; Tan and Wang 2020; Phillips et al. 2020; Zhang et al. 2020). Although some works have established the relationship among A, B, JRC, and the aperture e; however, these relationships cannot be degraded to the traditional cubic law when $\mathrm{JRC} = 0$, indicating that the relationships established are doubtful (Ni et al. 2018; Liu et al. 2020). Therefore, further lab tests are needed for the establishment of a reliable relationship between the coefficient A and B in the Forchheimer equation and the JRC, as well as the aperture e of rock fractures.

In addition, a great number of works have also been carried out on the numerical modeling of the seepage in fractured rock mass in the past decades. According to the ways of handling the seepage flow in fractures, three kinds of numerical methods or models widely used currently, they are (1) the equivalent seepage model; (2) the discrete fracture network seepage model; (3) the direct solution of Navier–Stokes equation. In the equivalent seepage model, the concept of Darcy's law in soil mechanics is introduced; and the fractured rock mass is treated as a continuum porous medium. An equivalent permeability is given to the fractured rock mass via the equality of water flux. The advantages of this model are that the basic theory is relatively simple and mature, and there are many solvers available. Moreover, it is much easier to be applied to large-scale (at the scale of

kilometers in size) engineering practice (Yifeng et al. 2010; Jackson et al. 2000). However, its shortcoming is that the equivalent permeability tensor of fractured rock mass needs to be estimated by the distribution of fractures network in a representative element volume (REV) (Liu et al. 2014; Yang et al. 2003). Since it is difficult to accurately investigate and characterize the distribution, connectivity, and geometric features of a fractures network in a REV in the practice, and there is a serious size effect for REV (Rong et al. 2013; Baghbanan and Jing 2008), thus the reliability of the estimated equivalent permeability generally is doubtful. When the distribution of fractures is relatively homogeneous, the estimation error for the seepage flux is generally in an acceptable range. However, when there are strong water-conducting fractures with a large aperture, and the distribution of fractures is uneven, the estimation of the water volume inflowing into tunnels and caverns may significantly differ from the reality.

The discrete fracture network seepage model assumes that the water can only flow in the fracture network; and the rock blocks are considered as the wall boundary (Ye et al. 2016; Jiang et al. 2013). This type of model can truly reflect the essential characteristic of how the fractures network controls the seepage in the rock mass. However, because the development of fracture network in rock mass is apparently complex, the computation will be very expensive. In the past decade, a series of meaningful works in this field have been conducted. For example, Baghbanan and Jing (2008), Min et al. (2004), and Jing et al. (2001) studied the influence of stress on the permeability of fractured rock mass by the DEM method. Liu et al. (2011) studied the equivalent permeability of rock mass which contains a random fractures network by adopting the UDEC package and the cubic law. Zhang and Wu (2010) proposed a 3D random fractures network seepage model and its solution method. Yan et al. (2015) developed a fluid–solid coupled model FDEM-Flow based on the cubic law. This model had been successfully applied to simulate the hydrofracturing problem of rock mass.

The traditional cubic law for the seepage in fractures is actually only applicable to the laminar flow. It is difficult to handle the roughness, irregular aperture, nonlinear flow, and local turbulence in an actual fractures network. To overcome the limitation of cubic law, the Navier–Stokes equation was numerically solved by many scholars to study the seepage in fractures (Zhao et al. 2018; Zhang et al. 2015; Liu et al. 2020). For example, Duan et al. (2013) solved the three-dimensional Navier–Stokes equation and found that the relationship between the aperture and flux was nonlinear. Liu et al. (2015) studied the nonlinear seepage characteristics in a crossed fractures network by solving the Navier–Stokes equation. Kosakowski and Berkowitz (1999) studied the variation characteristics of seeping flow at the crosses of fractures by solving the Navier–Stokes equation. Their numerical results indicated that natural fractures can produce a more complex seeping flow than those in artificial fractures. They also observed that the seeping flow at the crosses of fractures was disordered and presented nonlinear flow characteristics when the Reynolds number *Re* was in the range of 1–100. It was proved that it was necessary to incorporate the turbulence models in numerical simulation. Zhang et al. (2018) studied the unsaturated nonlinear two-phase seeping flow in a wide-aperture fractures network numerically. It was indicated by their results that the high-speed seeping process of the unsaturated water could be accurately and intuitively captured by solving the two-phase flow Navier–Stokes equation.

Summarily, abundant achievements have been obtained on the seepage characteristics in fractured rock mass, which have significantly promoted our recognition on the seepage characteristics in fractured rock mass. However, there are still some problems on the equations established in previous works for the relationship between the linear and nonlinear drag coefficients A, and B in the Forchheimer Equation and the aperture e, and the roughness JRC of fractures. In this study, taking the standard profile curves with their roughness JRC = 0–20 proposed by Barton and Choubey (1977), as well as the flat smooth curve (JRC = 0) as the base, a total of 44 transparent specimens each containing a single fracture with 11 different roughness and 4 different apertures (e = 1 mm, 1.25 mm, 2 mm and 2.5 mm) are first prepared by 3D-printing technique. Then, a series of seepage tests are performed to study the nonlinear seepage characteristics in a single rough fracture. Based on the experimental results, the relationships between the linear and nonlinear drag coefficients A, B in the Forchheimer equation, and the roughness JRC, the aperture e of fractures are established. Finally, a numerical simulation based on the Navier–Stokes equation is conducted to numerically study the seepage process and the typical characteristics in the 44 single rough fractures. It is indicated by the comparative analysis between the numerical and experimental results that the numerical simulation by solving the Navier–Stokes equation is a reliable method in the study of the seepage in single fractures.

2 Experiment Design

2.1 Specimen Preparation

The critical point of this experiment is on the production of these transparent specimens with different apertures and different roughness accurately. Due to the gradual maturity of the 3D-printing technique, it makes it is possible for us to produce these specimens with high quality. The preparation process is divided into the following four steps:

Step1: Taking the standard profile curves with different roughness (JRC = 0–20) proposed by Barton and Choubey (1977) as the base, the images of the 10 curves are, respectively, imitated adopting the software AutoCAD. Then 10 digital profile curves with 100 mm long, and with different roughness are obtained. To save the printing cost, the above 10 standard profile curves are all equally scaled-down, making the length of each profile curve becomes 60 mm. According to the work by Tse and Cruden (1979) and Yang et al. (2001), the equal scaling up or down for the fracture's profile will not change the value of JRC.

Step2: Through the software AutoCAD, 3D geometric models are established for the ten curves with different roughness (JRC = 0–20), as well as a perfectly smooth straight line (JRC = 0). First, the 2-dimensional fracture seepage channels are constructed for the 11 curves with different JRC by the way of parallel translation. The offset distance, i.e., the aperture e is 1 mm, 1.25 mm, 2 mm, and 2.5 mm, respectively. As a result, the roughness of the upper and lower boundaries of these fracture channels obtained is completely the same, avoiding the problem that the aperture is different along one fracture channel. The influence of this problem on the test data also can be eliminated. Second, these two-dimensional fracture seepage channels are all stretched by 10 mm on the third dimension (namely the fracture width w). Third, a 20 mm smooth section is respectively added to both sides of these fracture channels; and four screw threads with a diameter of 10 mm (Specification: DN6) used for inlet, outlet, and pressure taps are designed at the two lateral ends of these specimens, as illustrated in Fig. 1. Finally, the digital geometric models of 4 groups of the specimen with 4 different apertures and 11 different roughness are obtained.

Step 3: The electronic files with the format *.STL of each digital geometric model of fractures are all exported from AutoCAD, and then imported into 3D-printing controlling software.

Step 4: Since the minimum aperture of these specimens is 1 mm, to ensure the accuracy of these printed specimens, Stratasys J750 made in the USA with a print accuracy of 0.02–0.05 mm is selected as the printing equipment. The transparent resin produced by VeroClear is selected as the printing material. The upper and the lower part of the specimens are firstly printed; then they need to be grinded and polished for the purpose of transparency. Finally, the transparent upper and lower parts of these specimens are bonded together by glue.

2.2 Design of Test Equipment

Due to the fact that there is no purchasable equipment that can be directly used to perform the test involved in this study, we have to design and produce a piece of test equipment by ourselves for the seepage test of fractures. This test equipment includes a water tank, a peristaltic pump, a differential manometer, and a flow meter. The flux flowing through fractures can be controlled by adjusting the rotational speed of the peristaltic pump with an adjustable range of 0–100 rpm. The resolution for controlling the rotational speed is 0.1 rpm. The pressure pulse of the peristaltic pump can be reduced furthest via the principle of phase compensation. The measuring range of the differential manometer is 0 to 2500 Pa with an accuracy of 0.2%. The measuring range of the flowmeter is 5–500 mL/min with an accuracy of 0.25 mL/min.

After the water tank, peristaltic pump, fracture specimen, differential manometer, and the flow meter are connected adopting flexible hoses, a circulating water flow channel is formed. As a result, the water in the water tank can basically keep unchanged; and the influence of water level in the tank can be reduced. Before testing, each specimen should be firstly fixed horizontally. Then the peristaltic pump is adjusted to the maximum rotational speed for several minutes, making sure that all air and bubbles inside the fractures and flexible hoses are discharged, to ensure the seepage is saturated flow inside the fractures. During testing, the rotational speed of the peristaltic pump was manually adjusted to an appropriate value step by step. The water pressure difference between the two pressure taps, and the flowing flux through fractures are correspondingly recorded step by step by the differential manometer and the flow meter. Before this equipment produced by ourselves is used to perform the seepage test, it has been carefully calibrated by us, making sure the test data are reliable.

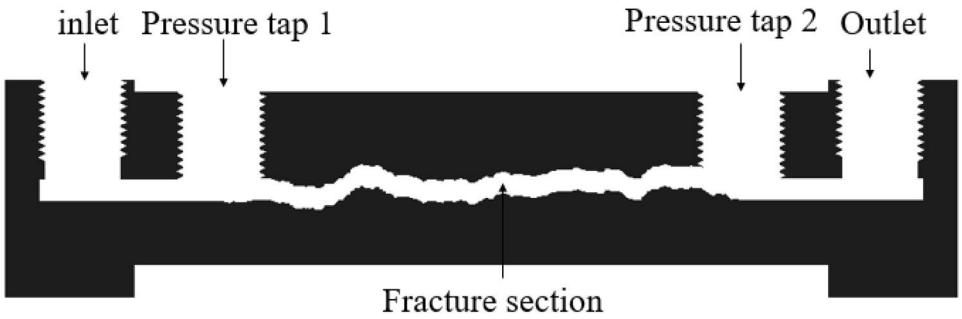

Fig. 1 A typical 3D digital geometrical model profile of the specimen with $e = 2.5$ mm and JRC = 18–20 (Thread specification: DN6)

3 Results and Analysis

3.1 Experimental Relationship of *q-I*

During tests, the room temperature in the laboratory is controlled at 25℃ through the air conditioning system (the hydrodynamic viscosity coefficient of water is $\mu = 0.9 \times 10^{-6}$ Pa·s at 25℃). The rotational speed of the peristaltic pump is adjusted step by step firstly from 0r/min to 100r/min with an interval of 5r/min, and then from 100r/min back to 0r/min also with the interval 5r/min. It is equivalent that parallel tests are conducted, which is conducive to ensure the reliability of test results. At each rotational speed, the reading of differential manometer ΔP and the reading of flowmeter Q (unit: m^3/s) are recorded, respectively, when the reading of the differential manometer and flowmeter become stable. According to the recorded Q and the ΔP, the seepage flux per unit width q and the hydraulic gradient I can be obtained through the following equation:

$$I = \Delta P/(\rho g \Delta L) \tag{1}$$

$$q = Q/w \tag{2}$$

where ρ is the density of water, g is the gravity, ΔL is the distance between the centers of the two pressure taps (it is 60 mm in this study), and w is the width of the fracture (it is 10 mm in this study). The flow speed U of water in fractures can be further determined by q/e.

Figure 2 illustrates the experimental relationship between the seepage flux per unit width q and the hydraulic gradient I for these 3D-printed fractures with 4 different apertures and 11 different roughnesses when q is within the range of $0–5.5 \times 10^{-4} m^2/s$. It is observed in Fig. 2 that the growth of hydraulic gradient I is nonlinear with q. Through mathematical matching, it is found that the relationship between q and I is a quadratic function, which satisfies the nonlinear permeability law proposed by Forchheimer in 1901:

$$I = Aq + Bq^2 \tag{3}$$

where A and B are the linear and nonlinear drag force coefficients. It can be seen in Fig. 2 that the correlation coefficient R^2 of these mathematical fitting generally are greater than 0.99, i.e., $R^2 > 0.99$. Based on the comparative analysis to the test data for the fractures with the same aperture, it is found that the hydraulic gradient I is positively related to the JRC of fractures under the condition of the same q. It is indicated that the greater the roughness is, the greater the resistance of fractures to the seeping water is, as well as the greater the energy dissipation of the seepage is, for the fractures with the same aperture. Based on the comparative analysis on the test data for the fractures with the same JRC, it is found that the hydraulic gradient I reduces significantly while the fracture aperture increases from 1 to 1.25 mm, 2 mm, and 2.5 mm under the condition of the same q. The reason is well known, that is the greater the aperture of fractures is, the less the resistance of fractures to the seeping water is.

The Reynolds number R_e is an important parameter to describe the flow characteristics of water in fractures. Reynolds number is generally defined as

$$R_e = \frac{\rho D U}{\mu} \tag{4}$$

where $\rho = 1000$ kg/m^3 is the water density, $\mu = 0.9 \times 10^{-6}$ Pa·s is the hydrodynamic viscosity coefficient of water at 25℃, D is the characteristic size of the flow. Due to the fact the seepage flow in the printed fractures is similar to the flow between two parallel flat plates, the characteristic size D can be determined as two times of the distance between the two parallel plates. Therefore, the characteristic size D should be $2e$ in this study. U is the flow speed, its relationship with q is $U = q/e$. Substituting $D = 2e$ and $U = q/e$ into Eq. (4), the Reynolds number can be formulated as

$$R_e = \frac{\rho D U}{\mu} = \frac{2\rho q}{\mu} = \frac{20q}{9} \times 10^9 \tag{5}$$

In Eq. (5), it seems that the Reynolds number has no relation with the aperture e of fractures if the Reynolds number is formulated by the seepage flux per unit width q in this study. Essentially, the Reynolds number is only dependent on the flow speed, characteristics size of structure, and the properties of fluids. Therefore, it should only have a very weak relationship with the roughness of fractures for the seeping flow involved in this study that is similar to the flow between two parallel flat plates. As illustrated in Fig. 2, the maximum seepage flux per unit width provided by the peristaltic pump is about $q_{max} = 5.5 \times 10^{-4} m^2/s$, the corresponding maximum Reynolds number is 1.22×10^6. Under this condition, the seeping flow in the printed fractures must be turbulent.

3.2 Validity of the Cubic Law for Smooth Fracture

Based on the comparative analysis to the test data for smooth fractures, as demonstrated in Fig. 2, it is observed that there is a linear relationship between q and I at a low seeping speed ($q < 1.5 \times 10^{-4} m^2/s$). In this study, a series of seepage tests at low seeping speeds are performed for the smooth fractures with four different apertures. The test results are shown in Fig. 3. It is observed that the hydraulic gradient I indeed grow linearly with q at the stage of low speed. It can also be found that the mathematical fitting results are generally coincident with the predicted result by the cubic law when the hydraulic gradient $I < 0.01$ for the smooth fractures with aperture $e = 1.25$ mm, 2 mm, and 2.5 mm.

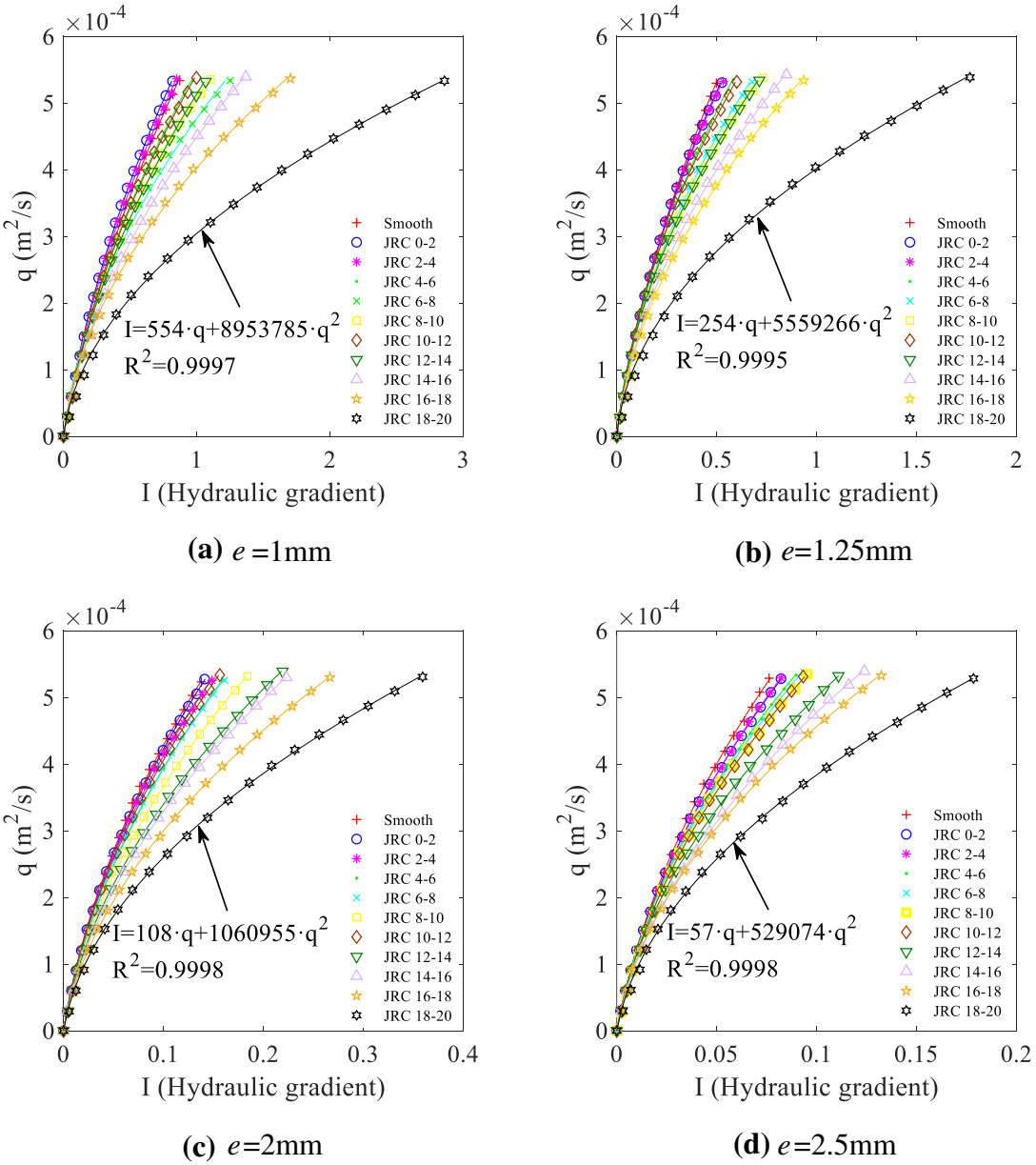

Fig. 2 Experimental relationship between the seepage flux per unit width q and the hydraulic gradient I (Noted: the discrete points are test data and continuous curve are fitted curves, and maximum Reynolds number $\mathrm{Re}=1.22\times10^6$)

However, for the smooth fracture with aperture $e=1$ mm, it is observed that there is an obvious deviation between the mathematical fitting result and the predicted result by the cubic law when $0.01<I<0.1$. Finally, it is indicated that the cubic law is applicable to the seepage in smooth fractures when $I<0.01$. In the case where $I>0.01$, the cubic law is not applicable; and the greater the I is, the larger the deviation will be between the cubic law and the experimental results.

3.3 Relationship Among the Linear Drag Coefficient *A* and JRC, *e*

Through the analysis to the test data, it has been confirmed that the Forchheimer equation Eq. (3) can accurately describe the q-I relationship for the seepage in rough fractures. In this section, a relationship between the linear drag coefficients A and JRC, e will be established. Based on the quantitative analysis for the linear coefficient A of the 44 fitting curves in Fig. 2 and the corresponding JRC and e, the relationship between A and JRC for the factures with four different apertures ($e=1$ mm, 1.25 mm, 2 mm, and 2.5 mm)

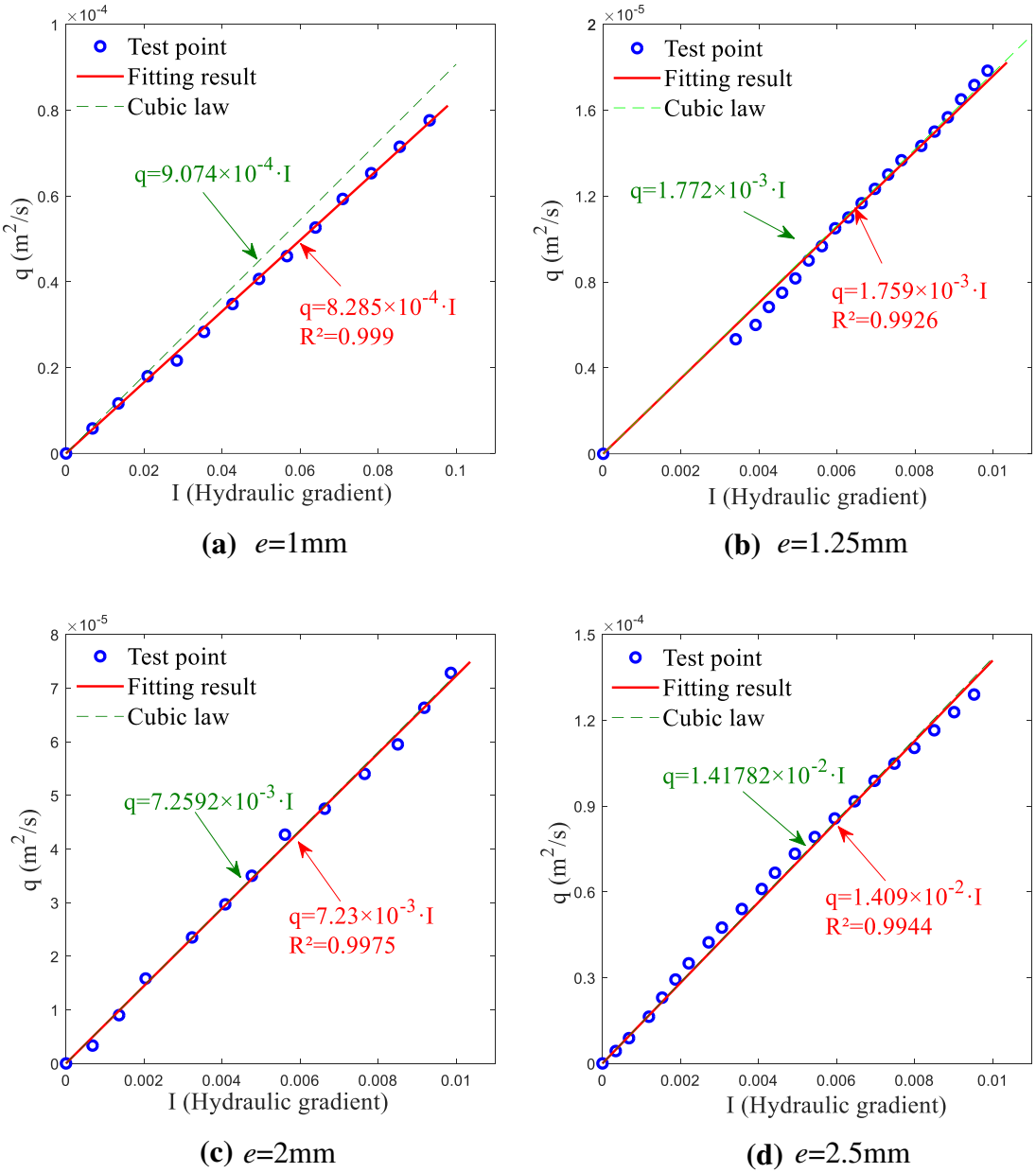

Fig. 3 Experimental relationship between q and the hydraulic gradient I at low-speed stage (JRC = 0)

are demonstrated in Fig. 4. It is observed that the linear coefficient A is negatively related to JRC when the aperture is small ($e = 1$ mm and 1.25 mm). It is indicated that great roughness has a significant influence on the linear resistance of fractures to seeping water when the aperture is small. For the fractures with a large aperture ($e = 2$ mm and 2.5 mm), it seems that there is no obvious relationship between the linear coefficient A and JRC. For instance, the linear coefficient A is in the range of 100–120 when $e = 2$ mm; and it is only in the range 50–64 when $e = 2.5$ mm. It is demonstrated that the roughness of fractures has little effect on the linear resistance of fractures to seeping water when the aperture is relatively large.

The relationship between the linear coefficient A and the fractures aperture e is illustrated in Fig. 5. It is observed in Fig. 5 that the discreteness of the value of A is large when the aperture is small ($e = 1$ mm or 1.25 mm); while the value of A is relatively concentrated when the aperture is large ($e = 2$ mm or 2.5 mm). For instance, A is in the range of 700–800 when $e = 1$ mm, and 350–450 when $e = 1.25$ mm; meanwhile, it is in the range of 100–120 when $e = 2$ mm, and 50–64 when $e = 2.5$ mm. Just as stated above, JRC has a great influence on A when the aperture is

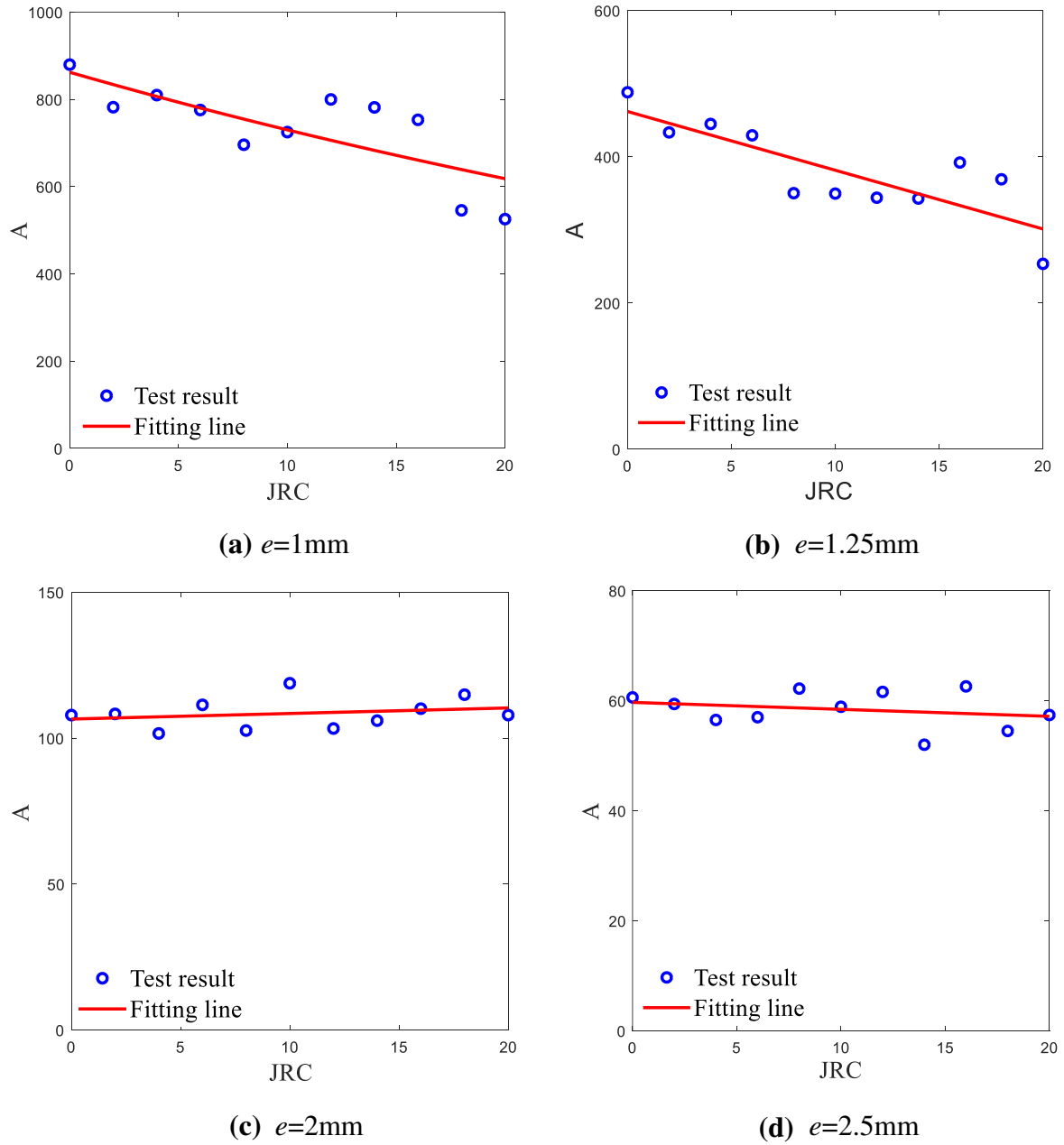

Fig. 4 Relationship curves of the linear drag coefficient A and the joint roughness coefficient JRC

small; while the effect of JRC on A is significantly weakened when the aperture is large. However, the effect of JRC is not taken into consideration in Fig. 5. Therefore, it is a quite normal phenomenon that the discreteness of the value of A is large when $e = 1$ mm or 1.25 mm in Fig. 5. Through mathematical fitting, it is found that the linear coefficient A is inversely proportional to the cubic power of fracture aperture e when JRC is the same, i.e. $A = C_A/e^3$, where C_A is a coefficient related to JRC, and its specific values are listed in Table 1. It is found that the correlation coefficients R^2 are all greater than 0.90, which means the reliability of data analysis is high. This regulation is similar to the cubic law.

If the 44 values of A, the corresponding JRC, and e are placed into the A-JRC-e three-dimensional space, then their spatial relationship can be obtained, as illustrated in Fig. 6. It is found that these data points can be generally described by a spatial curved surface in Fig. 6, and the equation of the spatial surface is:

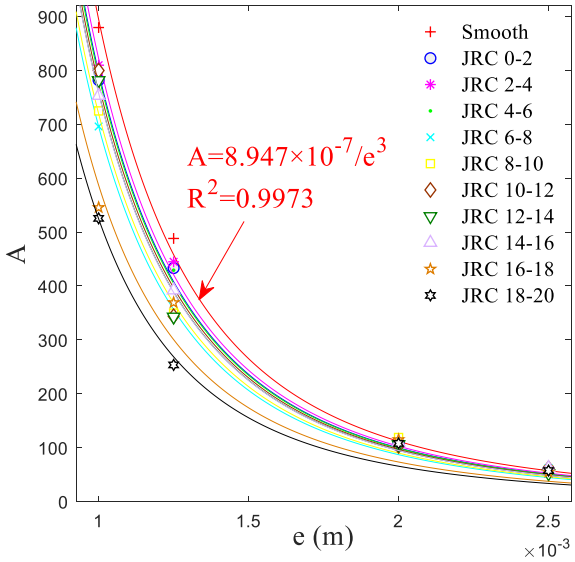

Fig. 5 Relationship curves of the linear drag coefficient A value and the aperture *e*

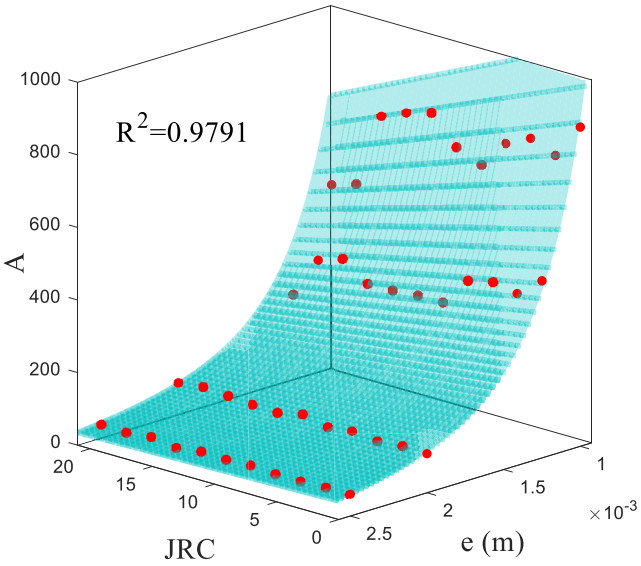

Fig. 6 Spatial curved surface for the relationship among the linear coefficient A and JRC, as well as the aperture *e*

Table 1 C_A value corresponding to different JRC and the corresponding R^2

JRC	C_A	R^2
Smooth	8.947×10^{-7}	0.9973
0–2	7.966×10^{-7}	0.997
2–4	8.221×10^{-7}	0.998
4–6	7.902×10^{-7}	0.9969
6–8	6.959×10^{-7}	0.9969
8–10	7.197×10^{-7}	0.9977
10–12	7.745×10^{-7}	0.9949
12–14	7.576×10^{-7}	0.9896
14–16	7.58×10^{-7}	0.9917
16–18	5.87×10^{-7}	0.946
18–20	5.246×10^{-7}	0.9805

$$A = \frac{-1.878\times10^{-6}\cdot JRC + 1.253\times10^{-4}}{144.2\cdot e^3} \tag{6}$$

It is shown in Fig. 6 that $R^2=0.9791$, indicating that the reliability of this spatial surface is high. Based on the form of Eq. (6), the general form of the relationship between *A* and JRC, *e* can be written as:

$$A = \frac{\mu}{ge^3}(a\cdot JRC + b) \tag{7}$$

where *a* and *b* are characteristic constants of fractures; *g* is the gravity, and μ is the dynamic viscosity coefficient of water. When JRC = 0, the above Eq. (7) can be degraded into the traditional cubic law.

It can be further confirmed in Fig. 6 that JRC has little effect on *A* when the aperture is large. However, as the fracture aperture gradually reduces, the value of A significantly increases. In this case, the influence of JRC on *A* becomes more and more significant.

3.4 Relationship Among the Nonlinear Drag Coefficient *B* and JRC, *e*

A similar method is taken to analyze the relationship among the nonlinear drag coefficient *B* and JRC, *e*. Figure 7 shows the relationship between *B* and JRC for the factures with four different apertures ($e=1$ mm, 1.25 mm, 2 mm, and 2.5 mm) are demonstrated in Fig. 7. As demonstrated in Fig. 7, the value of *B* is positively related to JRC; and the growth of *B* becomes faster with the increase of JRC. Through mathematical fitting, it is found that the mathematical relationship between *B* and JRC satisfy the following equation:

$$B = c\cdot \mathrm{JRC}^6 + d\cdot \mathrm{JRC} + f \tag{8}$$

where *c*, *d*, and *f* are three dimensionless parameters. It is observed that all the $R^2>0.90$ for the four different apertures. It is indicated that the reliability of Eq. (8) is good.

The relationship curves between *B* and the aperture of fractures *e* are illustrated in Fig. 8, where the different symbols represent the *B* values measured in tests when JRC is different, and the curves are mathematical fitting lines. It is observed that the nonlinear drag coefficient *B* is reduced with the increase of the aperture *e*. For the fractures with the same aperture, the greater the JRC is, the greater the value of *B* will be. Through mathematical fitting, it is found that the nonlinear drag coefficient *B* is inversely proportional to the cubic power of the aperture *e*,

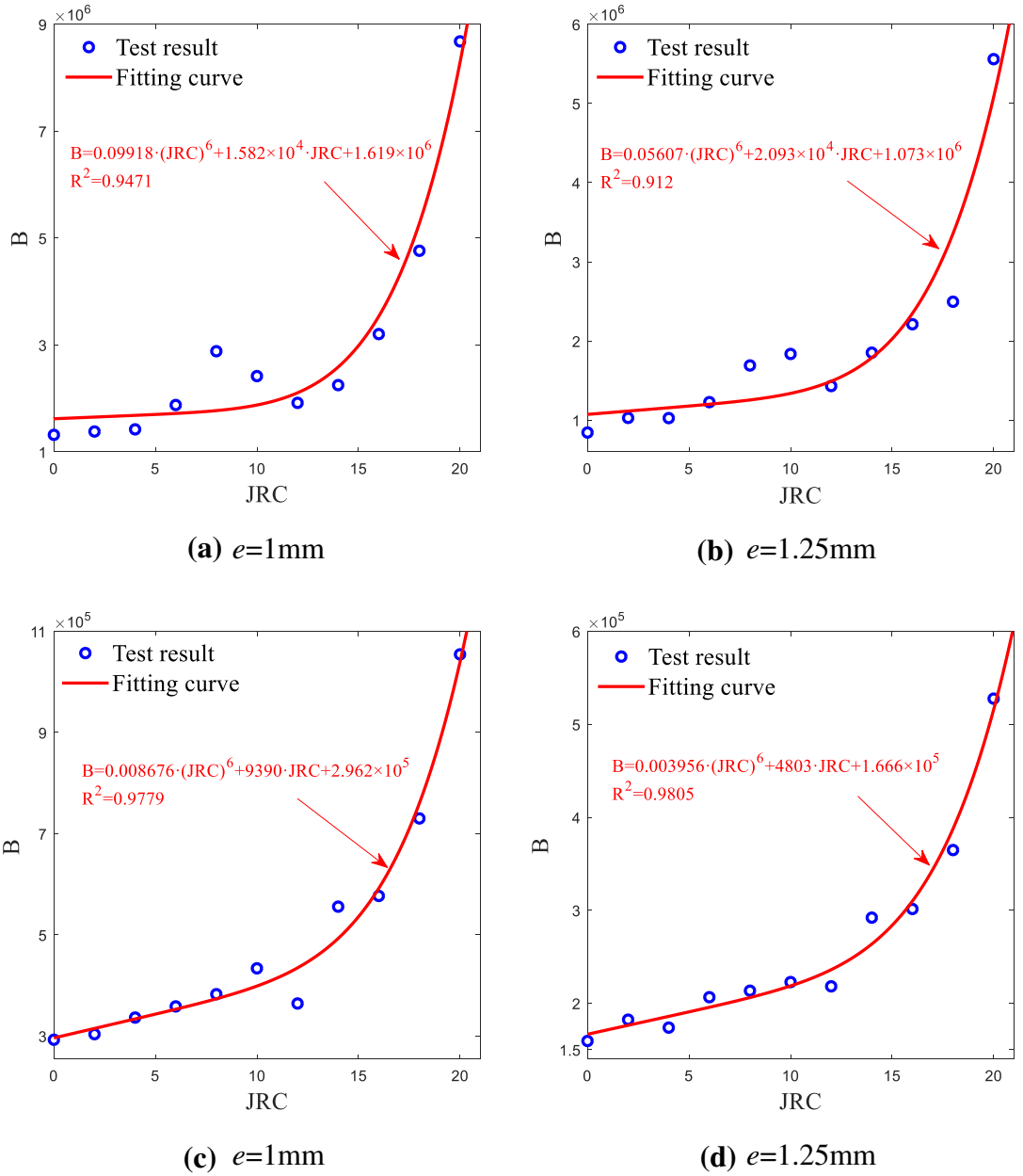

Fig. 7 Relationship curves of the nonlinear drag coefficient B and the joint roughness coefficient JRC

i.e., $B = C_B/e^3$, where C_B is the coefficient related to JRC, and its values are listed in Table 2. In Table 2, most of the correlation coefficient R^2 are greater than 0.90, indicating the correlation of the above fitting formula is very high.

If the 44 values of B, the corresponding JRC, and e are placed into the B-JRC-e three-dimensional space, then their spatial relationship can be obtained, as illustrated in Fig. 9. It is found that these data points can be generally described by a spatial curved surface, and the equation of the spatial surface is:

$$B = \frac{6.039 \times 10^{-10} \cdot JRC^6 + 4.693 \times 10^{-5} \cdot JRC + 1.055 \times 10^{-2}}{5.793 \cdot e^3} \tag{9}$$

It is shown in Fig. 9 that $R^2 = 0.9459$, indicating that the reliability of Eq. (9) is sufficient. Based on the form of Eq. (9), the general form of the relationship between B and JRC, e can be written as:

$$B = \frac{\mu}{ge^3}\left(c \cdot JRC^6 + d \cdot JRC + f\right) \tag{10}$$

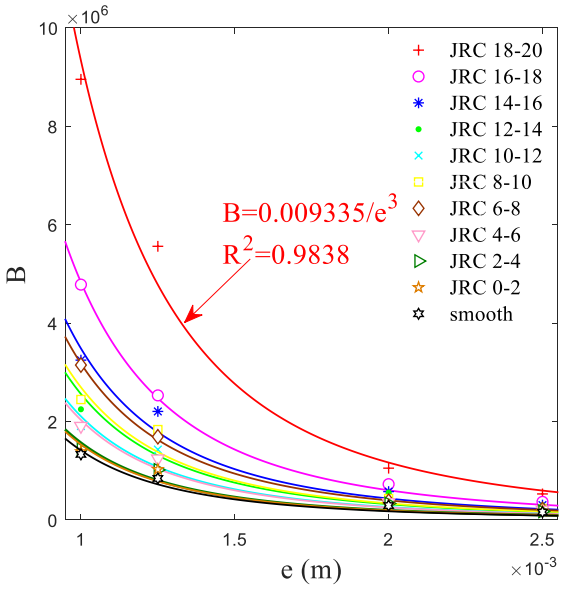

Fig. 8 Relationship curves of the nonlinear drag coefficient B value and the aperture *e*

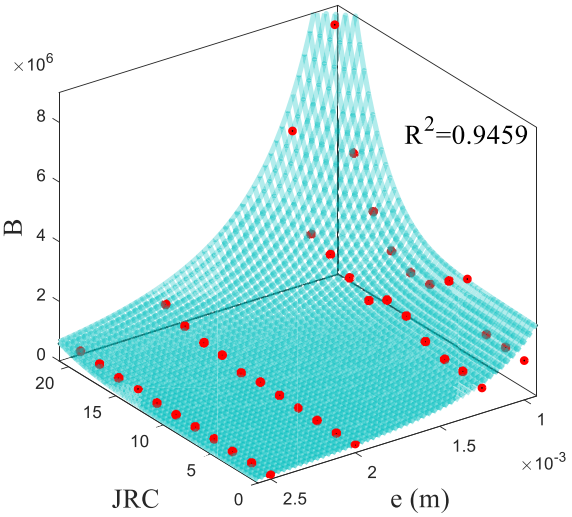

Fig. 9 Spatial curved surface for the relationship among the linear coefficient B and JRC, as well as the aperture *e*

Table 2 C_B value corresponding to different JRC and the corresponding R^2

JRC	C_B	R^2
Smooth	0.001414	0.9549
0–2	0.001534	0.9011
2–4	0.00157	0.9161
4–6	0.002032	0.9608
6–8	0.003179	0.999
8–10	0.002697	0.9194
10–12	0.002103	0.911
12–14	0.00256	0.8347
14–16	0.003486	0.9553
16–18	0.004831	0.998
18–20	0.009335	0.9838

where c, d, f are the characteristic constants of fractures. When JRC = 0, Eq. (10) is the same in form as the traditional cubic law. However, since the influence of nonlinear drag force is considered, Eq. (10) could describe high-speed seepage in smooth fractures.

It is observed in Fig. 9 that JRC has little influence on B when the aperture e is large. With the decreasing of the aperture e, JRC has a significant effect on the value of B. It is indicated that the resistance of fractures to seeping water increases with the fracture roughness. Especially, this effect will be very apparent when the aperture is small.

4 Numerical Simulation of the Seepage Flow in Single Rough Fracture

Except for physical lab tests, numerical simulation is also a very effective method to understand the seepage characteristics of fractures. In this section, the Navier–Stokes equation is solved to systematically study the seepage characteristics in a single rough fracture. The numerical results will be compared with the lab test results to verify the reliability of the numerical simulation. Furthermore, through numerical simulation computation, many mesoscopic seepage characteristics, such as boundary layer, streamline, etc., that cannot be observed in physical tests can be observed.

4.1 CFD Solver

In this study, the open-source CFD software platform OpenFOAM, is taken as the tool to simulate the seepage flow in a single rough fracture by solving the Navier–Stokes equation. The selected solver is PisoFOAM, which is a single-phase flow solver under the framework of OpenFOAM. It is mainly used to solve the motion characteristics of incompressible fluid. The governing equations for velocity and pressure are:

$$\nabla \cdot \vec{U} = 0 \tag{11}$$

$$\frac{\partial \vec{U}}{\partial t} + \nabla \cdot \left(\vec{U}\vec{U}\right) = -\frac{1}{\rho}\nabla P + \nabla \bullet \mu \nabla \vec{U} \tag{12}$$

where $\vec{U}$ represents the velocity vector, $\nabla = \frac{\partial}{\partial x}i + \frac{\partial}{\partial x}j + \frac{\partial}{\partial x}k$ represents the Hamiltonian operator, μ is the dynamic viscosity coefficient of water, P is the fluid pressure, ρ is the

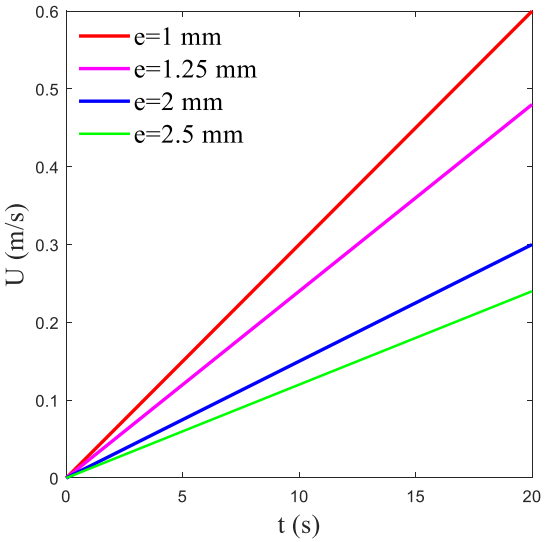

Fig. 10 Time history of the speed at the inlet of fractures

fluid density. In this study, the *k*-*ε* model is used to consider the influence of the turbulent models on the computational results.

4.2 Geometric Model of Fractures

To ensure the comparability between the numerical results and the above physical test results, the geometric model of fractures used in this section is completely consistent with that used in the physical tests, with 4 different apertures and 10 different roughness. The length of the geometrical model is 60 mm and the thickness is $(2+e)$ cm (completely the same as the 3D-printed fractures used in the physical tests). The fracture aperture e is also set as 1 mm, 1.25 mm, 2 mm, and 2.5 mm, respectively.

Computational mesh generation is performed in the seepage zone of fractures. The flow-velocity boundary U is applied at the left inlet of each fracture model, and the time history of the flow-velocity U at the inlet is demonstrated in Fig. 10. To ensure flowing flux at the inlet consistency with that in the physical tests (controlled by the peristaltic pump), the velocity at the inlet is inversely correlated with the aperture of fractures. The total simulation time is set as the 20 s in computation. The fluid is assumed to be pure water at 25 ℃, with a density of 1000 kg/m^3 and a dynamic viscosity coefficient of 0.9×10^{-6} Pa·s. Due to the influence of roughness, the seeping flow in fractures is generally turbulent flow. To study the influence of the *k*-*ε* turbulence model is used or not in computation, the seeping flow in the 40 rough fractures without considering the turbulent model is also simulated in this study. For the cases in which no turbulent model is used, we call the seeping flow as laminar flow thereafter.

4.3 Numerical Relationship of *q*-*I*

A series of CFD simulations are performed for the 40 rough single fractures with different apertures and JRC in which a turbulent model is used or not used. From the computational results, the water pressure and velocity at the time $t=0$, 2, 4, 6…, and 20 s at the midpoint of the inlet and outlet of fracture models are first extracted. Then, the numerical relationship of *q*-*I* can be obtained by applying Eqs. (1) and (2). Figures 11, 12 are the numerical relationship of *q*-*I* for single fractures where a turbulent model is used or not used, respectively.

In Figs. 11 and 12, the discrete points are the numerical results; and the continuous lines are the mathematical fitting lines where the correlation coefficients R^2 are all greater than 0.9. It is indicated by the numerical results that the seeping flow in single rough fractures also can be described by the Forchheimer Eq. (3), regardless of the turbulence model is used or not. It means that the hydraulic gradient I increase nonlinearly with q. For the fractures with the same aperture, the nonlinearity of the hydraulic gradient I become stronger and stronger with the increasing of fracture roughness. These characteristics are completely consistent with the rules revealed by the physical tests performed by us.

4.4 Comparison Between Numerical Results and Test Results

To compare the test results and numerical results more intuitively, the fractures with JRC = 0–2 or JRC = 18–20, and with four different apertures are selected as the typical representatives, to demonstrate the reliability of numerical simulation in which the Navier–Stokes equation is solved. The comparisons between the numerical results and test results are illustrated in Figs. 13, 14.

It can be seen in Figs. 13, 14 that the numerical results based on the Navier–Stokes equation are not completely the same as the test results. The deviation between them is tiny in some cases, for example, the numerical results are generally consistent with the test results when JRC = 18–20, $e=2$ mm or $e=2.5$ mm. However, the deviation is quite significant in some cases, for instance, there is a large gap between the numerical results and the test results when JRC = 18–20 and $e=1$ mm. This deviation may be caused by the printing error on the physical specimen, as well as the inaccuracy of the description of the discreted meshes on the rough boundaries of fracture in the numerical model. This effect is weak when the aperture is large, but this effect is very significant when the aperture is small. Therefore, the mesh discretization on the rough boundaries of fractures

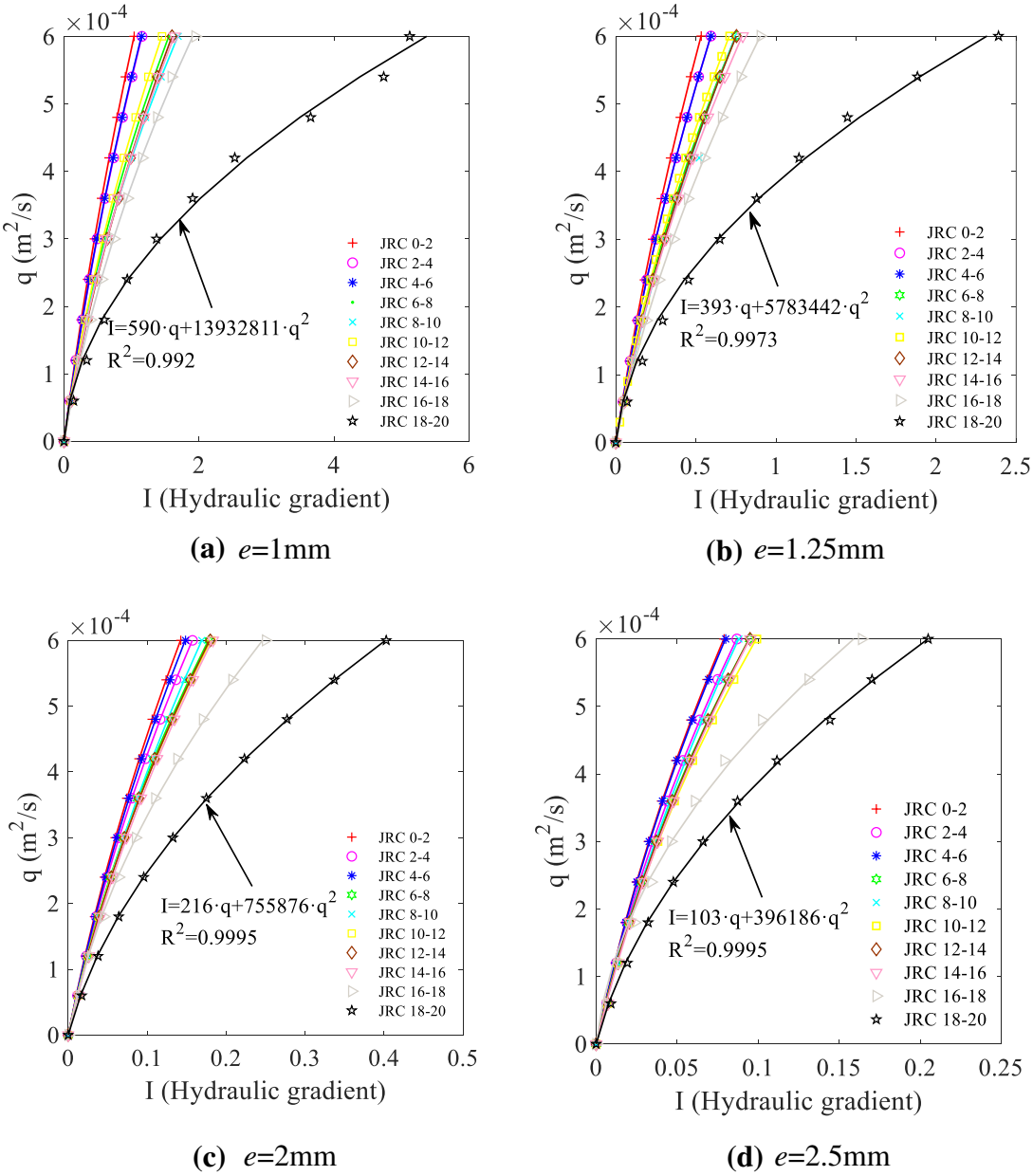

Fig. 11 Numerical results of *q*-*I* relationship for the flow in single rough fracture (Laminar flow)

must be very fine when carrying out the numerical simulation for the fractures with small aperture. Only in this way can the reliable results be obtained. In some cases, when the flow speed is low, the numerical results are consistent with the test results; however, when the flow speed is high, the gap between them is more and more significant for the same fracture, as demonstrated in Fig. 13(c, d). Finally, it is observed that there are some differences, but not significant between the numerical results, regardless of the *k*-ε turbulent model is used or not.

In general, there is good comparability and consistency between the numerical results and the test results. It proves that the numerical simulation by solving the Navier–Stokes equation can be considered as a reliable method in the study of fracture seepage.

4.5 Seepage Velocity Field in Single Rough Fracture

Taking the fractures with the aperture $e = 1$ mm as the typical case, Fig. 15 shows the speed field obtained by the numerical simulation for the fractures without using the

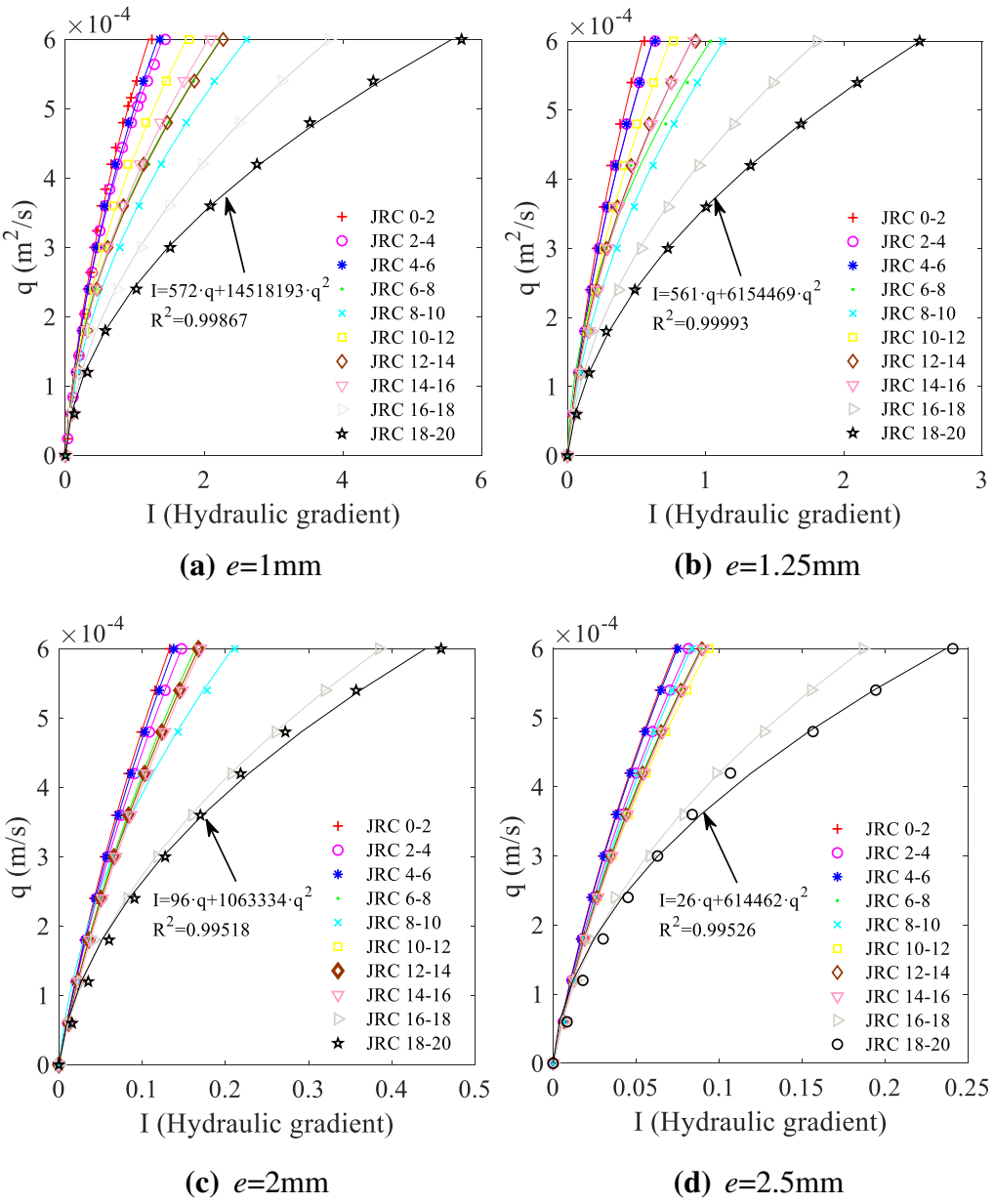

Fig. 12 Numerical results of *q*-*I* relationship for the flow in single rough fracture (Turbulent flow)

turbulent model when $e = 1$ mm. It can be seen in Fig. 15 that the distribution characteristics of the speed in all rough fractures are that the speed in the zone near to the upper and lower boundaries of fractures is low; while it is high in the middle zone. There is the typical boundary layer structure. It is known that the flow speed at the left inlet is 0.6 m/s; while the maximum seeping speed are all greater than 0.6 m/s in the fractures with different roughness, for example, the maximum speed in fractures are 0.9962 m/s, 1.017 m/s, 1.0114 m/s, 1.2365 m/s, 1.3079 m/s, 1.1087 m/s, 1.7978 m/s, 1.276 m/s, 1.5403 m/s, and 1.9268 m/s, respectively corresponding to JRC = 0–2, JRC = 2–4,…,and JRC = 18–20. The amplification is all more than 60%; especially, the maximum seeping speed is 3.2 times of the velocity at the inlet when JRC = 18–20.

Figure 15 also shows that the roughness has a significant influence on the seepage flow in fractures. When the aperture and the speed at the inlet are the same, the rougher the fracture surface is, the greater the thickness of the boundary layer will be. Moreover, due to the great variety of the topography of fractures, the rougher the fractures are, the greater the resistance of fractures to the seeping water will be, leading to a positive correlation between the maximum flow speed and the JRC.

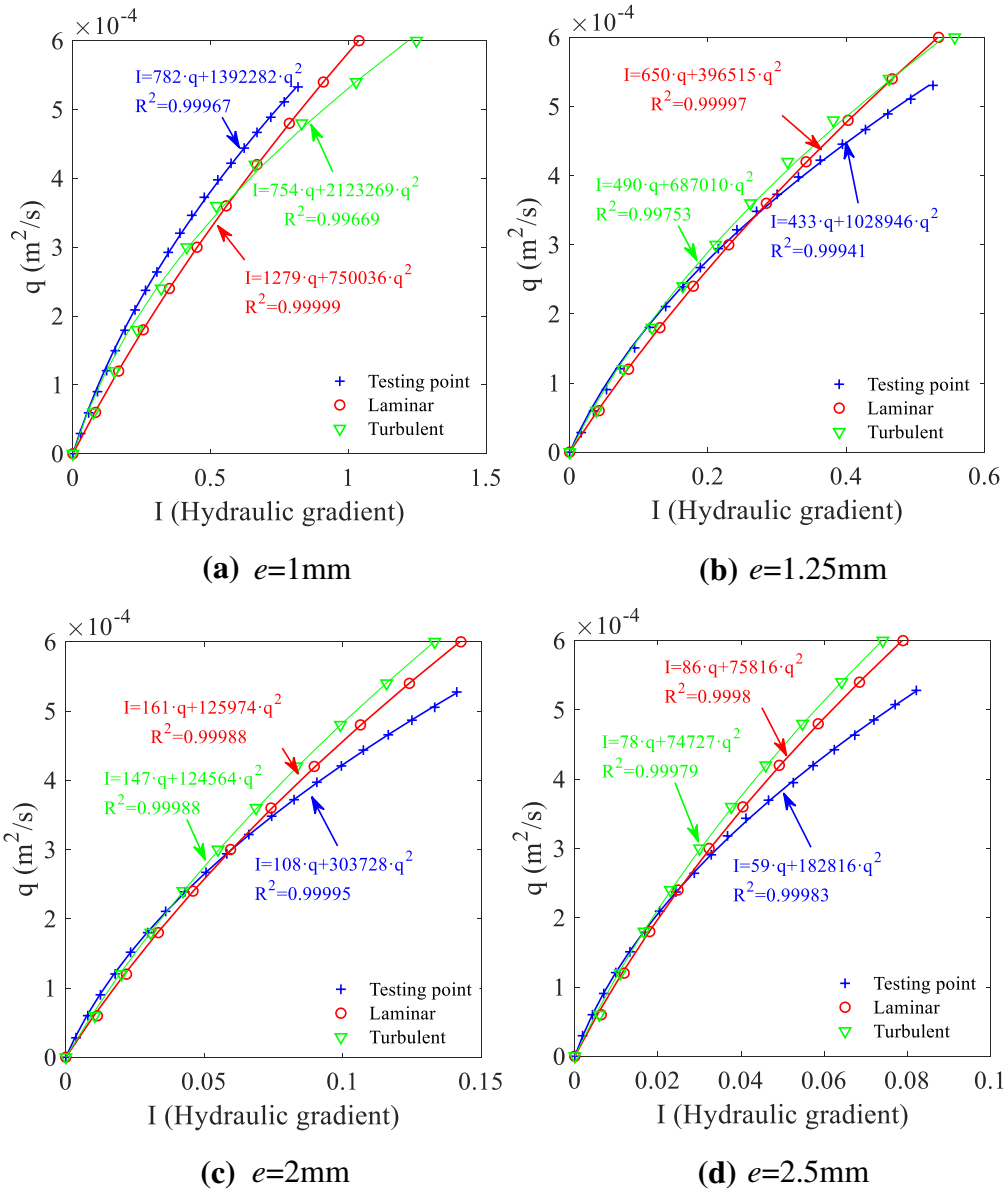

Fig. 13 Comparison of the *q*-*I* relationship between the numerical results and test results when JRC = 0–2

Figure 16 shows the flow speed field obtained by the numerical simulation in which the *k*-*ε* turbulence model is used for the fractures with $e = 1$ mm. When JRC = 0–2, JRC = 2–4, …, and JRC = 18–20, the corresponding maximum speed is 0.9822 m/s, 1.0098 m/s, 0.9879 m/s, 1.1801 m/s, 1.239 m/s, 1.0832 m/s, 1.1224 m/s, 1.0979 m/s, 1.1247 m/s, and 1.2392 m/s, respectively. For the same inlet speed 0.6 m/s, the amplification of the flow speed in these fractures ranges from 63.7 to 106.5% if the *k*-*ε* turbulence model is used in the computation. Compared with Fig. 15, it can be found that the maximum seeping speed in fractures adopting turbulence model is less than that if no turbulence model is used. From the physical perspective, due to the influence of roughness, the high-speed seeping in fractures is impossible to be laminar flow but should be turbulent flow. Therefore, the maximum seeping speed in fractures will be seriously overestimated if no turbulence model is used in the numerical simulation. Based on this recognition, the numerical results without turbulence model will not be analyzed thereafter.

Besides the influence of JRC, it is also necessary to further explore the influence of aperture on the seepage speed field in the fractures with the same JRC. Here, the fractures with JRC = 18–20 are taken as the typical representative to conduct such a study. Figure 17a shows the seepage speed

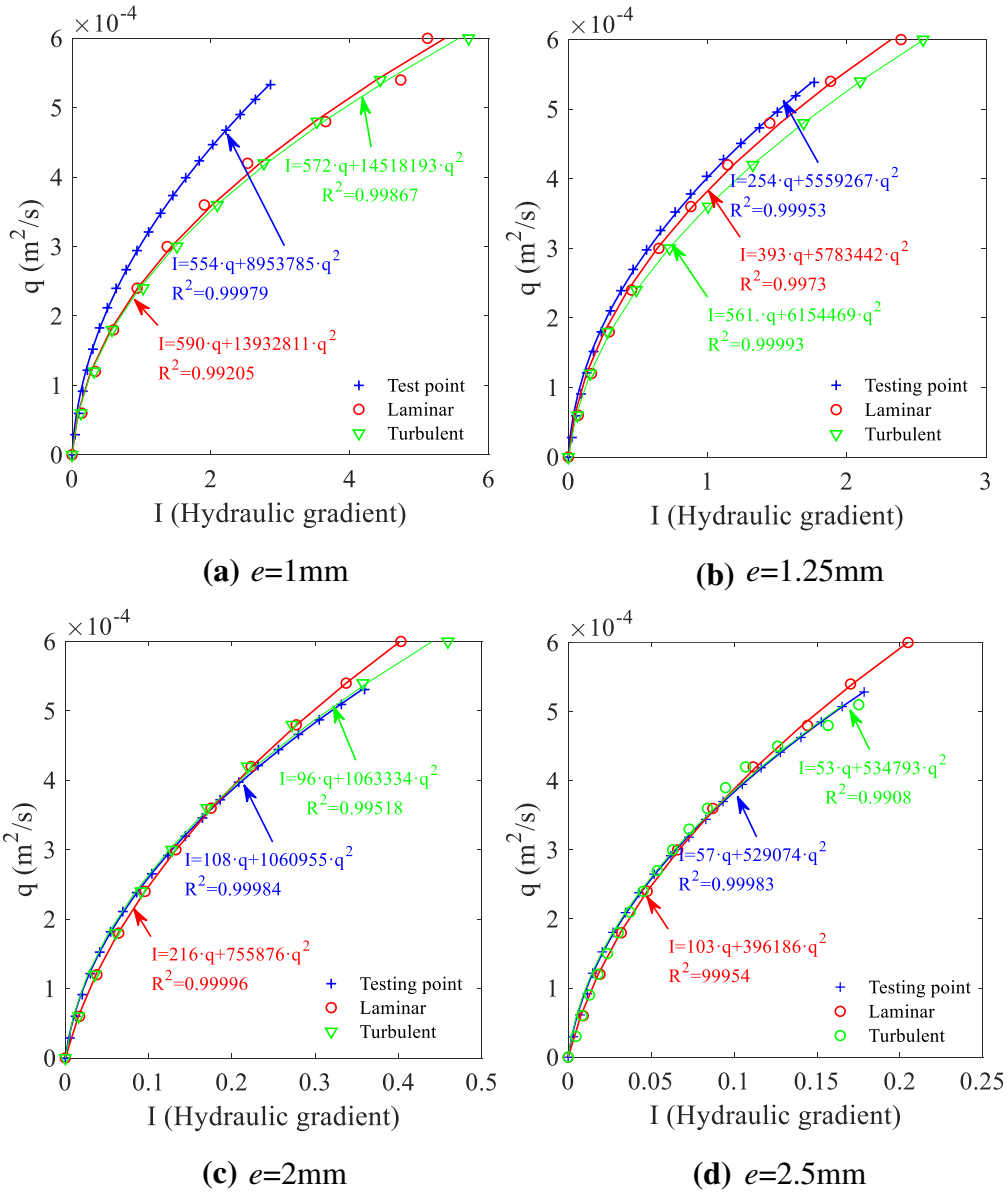

Fig. 14 Comparison of the *q*-*I* relationship between the numerical results and test results when JRC = 18–20

fields in the fractures with four different apertures when JRC = 18–20 where a turbulent model is used. To be consistent with the physical tests, the same seepage flux per unit width q is applied at the inlets of the four different fractures. As a consequence, the speeds at the inlets of the four fractures are different; they are, respectively, set as 0.6 m/s, 0.48 m/s, 0.3 m/s, and 0.24 m/s in computation.

The numerical results show that there are also two low-speed zones near the upper and lower fracture boundaries, and the speed is relatively high in the middle zone of fractures. There is also a typical boundary layer structure. The maximum seeping speed in the four fractures with different apertures are 1.2392 m/s, 1.0755 m/s, 0.6107 m/s and 0.4714 m/s, respectively. Compared with the speed at the inlet, it is amplified by 106.5%, 124%, 103.6%, and 96.4%, respectively. It is known that the amplification of the maximum seeping speed relative to the inlet speed is negatively related to the apertures. It is indicated that the seeping resistance applied by boundary layers is reduced with the increasing of the aperture, because the sectional area passable for water becomes larger for the fractures with the same JRC. Certainly, the maximum speed also correspondingly becomes smaller.

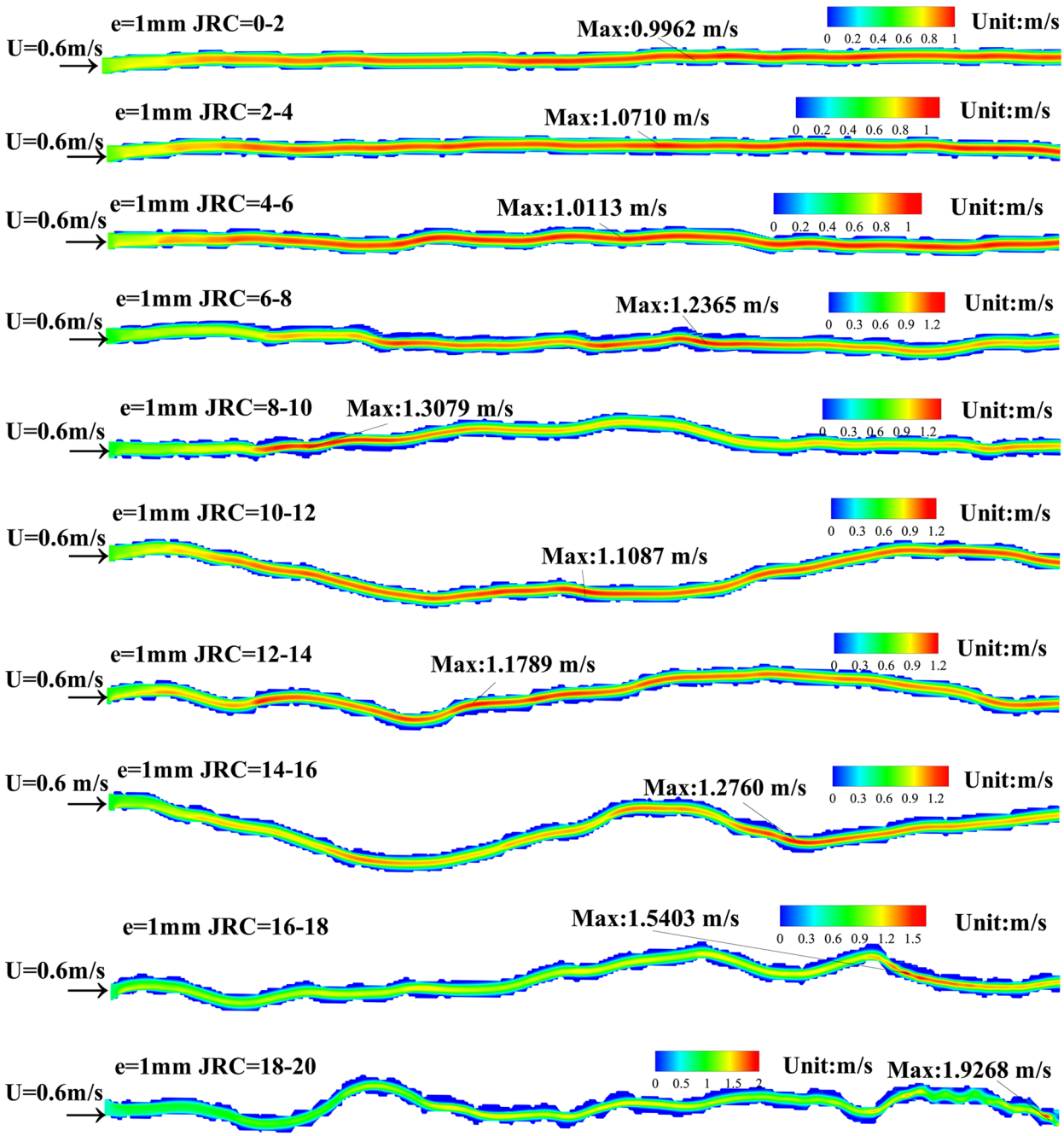

Fig. 15 Numerical results of the seepage speed field in the fractures with $e = 1$ mm (Laminar flow)

4.6 Seepage Pressure Field in Single Rough Fracture

In this part, the distribution characteristics of seepage pressure field in rough single fractures, as well as the influence of JRC, aperture e of fractures on the pressure field will be studied. Figure 18 shows the distribution of the seepage pressure field in the fractures with various roughness when $e = 1$ mm.

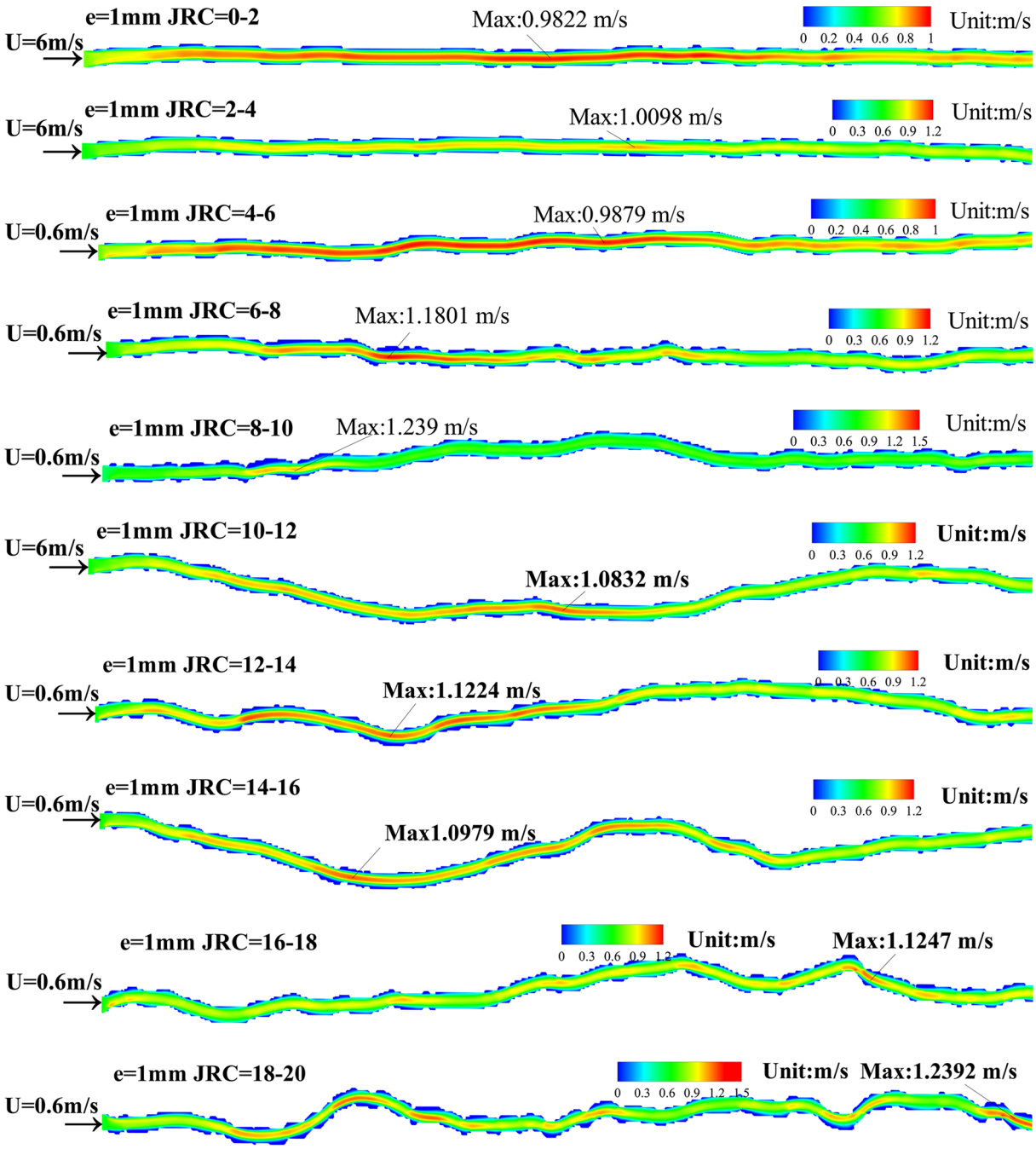

Fig. 16 Numerical results of the seepage speed field in the fractures with $e = 1$ mm (Turbulent flow)

It can be seen in Fig. 18 that the maximum water pressure generally appears at the inlets of the fractures. The pressure distribution is gradually reduced to 0 Pa at the outlet along the flowing direction. The pressure values at the midpoint of the inlet and outlet of fractures are extracted. It is found that the difference of pressure at the two ends of these fractures is 733.4 Pa, 846 Pa, 800.8 Pa, 1304.3 Pa, 1537 Pa, 1049.6 Pa, 1337.9 Pa, 1234.8 Pa, 2237.1 Pa, 3358.6 Pa, respectively. It can be found that the pressure difference between the two ends of fractures gradually increases with JRC. It is indicated that the fractures with large roughness have great resistance to the seeping water. The energy consumption is correspondingly considerable in the seeping process.

Taking the fracture with JRC = 18–20 as the typical example, the influence of aperture on the seepage pressure field is studied. The numerical results are shown in

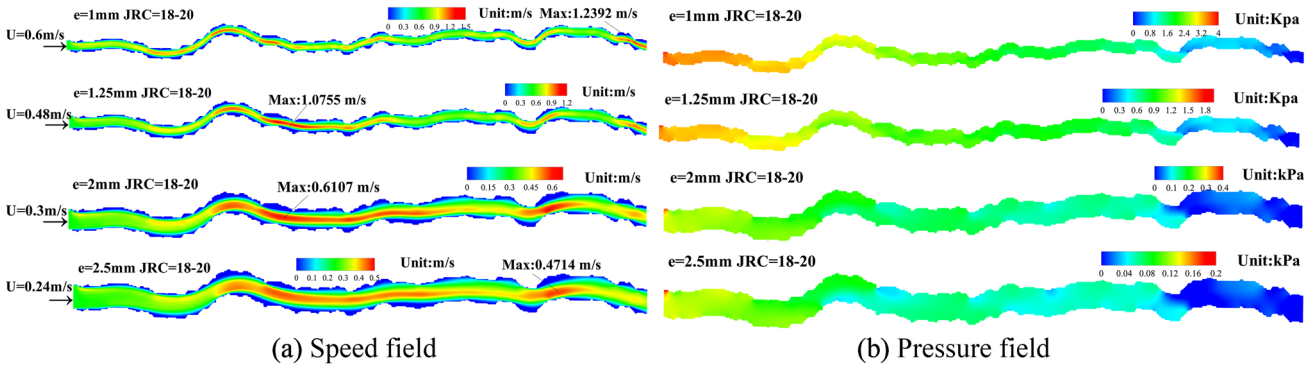

Fig. 17 Numerical results of the seepage speed field, and the pressure field in the fractures with different apertures when JRC = 18–20 (k-ε model is used)

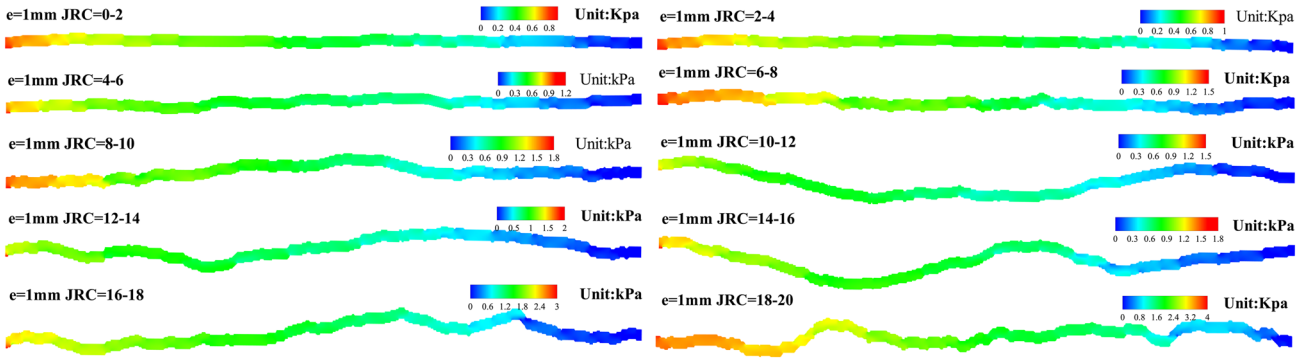

Fig. 18 Numerical results of the seepage pressure field in the fractures with various JRC when $e = 1$ mm (k-ε model is used)

Fig. 17b. After the pressure at the middle point of the inlet and outlet of fractures are extracted, it is known that the pressure difference at the inlet and outlet are 3358.6 Pa, 1498.2 Pa, 270 Pa, and 141.7 Pa, respectively, when the aperture $e = 1$ mm, 1.25 mm, 2 mm, and 2.5 mm. It is shown that the pressure difference between the inlet and outlet of the fractures reduces sharply with the aperture e. This result shows that the fracture aperture has a significant negative correlation with the seepage pressure difference.

5 Conclusion

In this study, a series of transparent specimens with a single rough fracture are produced by the 3D-printing technique, by which the aperture and joint roughness of fractures are accurately controlled. To conduct the seepage test for these printed fractures, a piece of test equipment is specially designed and made. Taking this designed test equipment as the experimental platform, a series of seepage tests are performed. Through the analysis to the physical test results and numerical results, the following four recognitions are obtained:

(1) Through the seepage tests, it is further confirmed that the relationship between the seepage flux per unit width q and the hydraulic gradient I of single rough fractures satisfy the nonlinear relationship described by the Forchheimer equation.

(2) Through the seepage tests for the fractures with different apertures involving low seeping velocity ($q < 1.5 \times 10^{-4} \mathrm{m}^2/\mathrm{s}$), it is found that the cubic law is only applicable to the seepage in smooth fracture when the hydraulic gradient $I < 0.01$. When $I > 0.01$, the cubic law is no longer applicable, and the greater the hydraulic gradient I is, the greater the deviation between the cubic law and the test data is.

(3) Based on the analysis to the drag coefficients A and B in the Forchheimer equation, which are determined by the mathematical fitting for the seepage test data, the general relationship between drag coefficients A and B, JRC, and the aperture e is established as:

$$A = \frac{\mu}{ge^3}\left(a \cdot JRC + b\right)$$

$$B = \frac{\mu}{ge^3}\left(c \cdot JRC^6 + d \cdot JRC + f\right)$$

where a, b, c, d, and f are the physical parameters of fractures, e is the aperture, μ is the fluid viscosity coefficient, and g is the gravity. Since the above two relationships are established based on the test data for which the aperture of fracture $e \geq 1$ mm, currently, it is hard to say that the above two relationships are universally applicable to the fractures with a tiny aperture, e.g. 10 µm. More works are needed to answer this question in the future.

(4) Taking the open-source software OpenFOAM as the computational platform, a series of numerical simulations are conducted for the fractures models that are completely the same as that used in the physical tests, in which turbulent model is used or not. Based on the numerical results, it is found that there is a typical boundary layer structure on the profile of fractures for seepage flow; and the numerical results are in good agreement with the physical results. For high-speed seepage, it is recommended to use a turbulence model in computation. Otherwise, the flow velocity in fractures would be significantly overestimated. The numerical results show that JRC and the aperture e of fractures have a significant influence on the distribution of the seepage speed field and pressure field. Finally, it is indicated by the numerical simulation presented in this study that the way by solving the Navier–Stokes equation is also a reliable method to study the seepage in fractures and useful addition to the physical testing.

Acknowledgements We sincerely appreciate the financial support from the National Natural Science Foundation of China, Project No. 51879257.

Reference

Amadei B, Illangasekare TA (1994) Mathematical model for flow and solute transport in nonhomogeneous rock fracture. Int J Rock Mech Mining Sci Geomech Abst 18:719–731

Baghbanan A, Jing LR (2008) Stress effects on permeability in a fractured rock mass with correlated fracture length and aperture. Int J Rock Mech Mining Sci Geomech Abst 45(8):1320–1334

Barton N, Choubey V (1977) The shear strength of rock joints in theory and practice. Rock Mech 10:1–54. https://doi.org/10.1007/bf01261801

Barton N, Bandis S, Bakhtar K (1985) Strength deformation and conductivity coupling of rock joints. Int J Rock Mech Mining Sci Geomech Abst 22(3):121–140

Chen YF, Zhou JQ, Hu SH, Hu R, Zhou CB (2015) Evaluation of Forchheimer equation coefficients for non-Darcy flow in deformable rough-walled fractures. J Hydrol 529:993–1006

Duan MB, Li G, Meng YF, Ma X, Li HT (2013) Research on regulation of fracture seepage in different joint roughness coefficients. J Water Res Water Eng 24(5):41–44

He YL, Tao YJ, Yang LZ (2010) Experimental research on hydraulic behaviors in a single joint with various values of JRC. Chin J Rock Mech Eng 29(Supp. 1):3235–3241

Jackson CP, Hoch AR, Todman S (2000) Self-consistency of a heterogeneous continuum porous medium representation of a fractured medium. Water Resour Res 36(1):189–202

Jiang QH, Yao C, Ye ZY, Zhou CB (2013) Seepage flow with free surface in fracture networks. Water Resour Res 49:176–186

Jing LR, Ma Y, Fang ZL (2001) Modeling of fluid flow and solid deformation for fractured rocks with discontinuous deformation analysis (DDA) method. Int J Rock Mech Min Sci 38(3):343–355

Kosakowski G, Berkowitz B (1999) Flow pattern variability in natural fracture intersections. Geophys Res Lett 26(12):1765–1768

Liu QS, Wu YX, Liu B (2011) Discrete element analysis of effect of stress on equivalent permeability of fractured rockmass. Chin J Rock Mech Eng 30(1):176–183

Liu RC, Jiang YJ, Li B, Wang XS, Xu BS (2014) Numerical calculation of directivity of equivalent permeability of fractured rock masses network. Rock and Soil Mechanics 35(8):2394–2400

Liu RC, Jiang YJ, Li SC, Li B, Wang XS (2015) Study of nonlinear hydraulic characteristics and hydraulic aperture calculation of crossed fracture. Rock Soil Mech 36(6):1581–1590

Liu XS, Li M, Zeng ND, Li T (2020) Investigation on nonlinear flow behavior through rock rough fractures based on experiments and proposed 3-dimensional numerical simulation. Geofluids. https://doi.org/10.1155/2020/8818749

Lomize GM (1951) Flow in fractured rocks. Gosemergoizdat, Moscow

Louis C (1974) Rock hydraulics in rock mechanics. Springer, New York

Min KB, Rutqvist J, Tsang CF, Jing LR (2004) Stress-dependent permeability of fractured rock masses: a numerical study. Int J Rock Mech Mining Sci 41(7):1191–1210

Ni XD, Niu YL, Wang Y, Yu K (2018) Non-darcy flow experiments of water seepage through rough-walled rock fractures. Geofluids. https://doi.org/10.1155/2018/8541421

Patir N, Cheng HS (1978) An average flow model for determining effect of three-dimensional roughness on partial hydrodynamic lubrication. J Lubr Technol 100(1):12–17

Phillips T, Bultreys T, Bisdom K, Kampman N, Van Offenwert S, Mascini A, Cnudde V, Busch A (2020) A systematic investigation into the control of roughness on the flow properties of 3d-printed fractures. Water Resour Res. https://doi.org/10.1029/2020WR028671

Rong G, Peng J, Wang X, Liu G, Hou D (2013) Permeability tensor and representative elementary volume of fractured rock masses. Hydrogeol J 21:1655–1671

Su B, Meili Z, Jian Z (1995) Study on fracture seepage in the imitative nature rock. Chin J Geotech Eng 17(5):19–24

Tan WH, Wang PF (2020) Experimental study on seepage properties of jointed rock-like samples based on 3D printing techniques. Adv Civil Eng. https://doi.org/10.1155/2020/9403968

Tian ZG, Dai CQ, Zhao QS, Meng ZB, Zhang BL (2021) Experimental study of joint roughness influence on fractured rock mass seepage. Geofluids 2021:8813743. https://doi.org/10.1155/2021/8813743

Tse R, Cruden DM (1979) Estimating joint roughness coefficients. Int J Rock Mech Min Sci Geomech Abstr 16(5):303–307

Wang Y, Su BY (2002) Research on the behavior of fluid flow in a single fracture and its equivalent hydraulic aperture. Adv Water Sci 13(1):61–68

Wang PF, Tan WH, Ma XW, Li ZJ, Liu JJ, Wu YF (2019) Experimental study of seepage characteristics of consecutive and filling fracture

with different roughness levels and gap-widths. Rock Soil Mech 40(8):3062–3070
Xu GX, Zhang YX, Ha QL (2003) Super cubic and sub cubic law of rough fracture seepage and its experiments study. J Hydraul Eng 34(3):74–79
Yan CZ, Zheng H, Sun GH, Ge XR (2015) A 2D FDEM-flow method for simulating hydraulic fracturing. Chin J Rock Mech Eng 35(1):67–75
Yang ZY, Lo SC, Di CC (2001) Reassessing the joint roughness coefficient (JRC) estimation using Z2. Rock Mech Rock Eng 34(3):243–251
Yang TH, Zhang YB, Leng XF, Tang CA (2003) Tensor analysis of seepage flow from structural plane network of rock mass. J Northeastern Univ Nat Sci 24(9):911–914
Ye ZY, Jiang QH, Zhou CB, Liu YZ (2016) Numerical analysis of unsaturated seepage flow in two dimensional fracture networks. Int J Geomech 17:04016118
Yifeng C, Chuangbing Z, Mao Xinying HR (2010) Numerical simulation and assessment of seepage control effects on surrounding rocks of underground powerhouse in Shuibuya hydropower project. Chin J Rock Mech Eng 29(2):308–318
Zhang Z, Nemcik J (2013) Fluid flow regimes and nonlinear flow characteristics in deformable rock fractures. J Hydrol 477(1):139–151
Zhang QH, Wu AQ (2010) Three-dimensional arbitrary fracture network seepage model and its solution. Chin J Rock Mech Eng 29(4):720–730
Zhang QG, Ju Y, Gong WB, Zhang L, Sun HF (2015) Numerical simulations of seepage flow in rough single rock fractures. Petroleum 1:200–205
Zhang Y, Zhou X, Ye JH (2018) Numerical analysis of nonlinear two-phase flow within large opening fracture networks in rockmass. Chin J Rock Mech Eng 37(4):931–939
Zhang S, Qiao WG, Wu Y, Fan Z, Zhang L (2020) Experimental study on seepage characteristics of microfracture with different aperture. Sci Rep 10:5452
Zhao K, Wang HL, Xu WY, Xia J (2017) Experimental study on seepage characteristics of rock-like materials with consecutive and filling fractures. Chin J Geotech Eng 39(6):1130–1136
Zhao JH, Yin LM, Guo WJ (2018) Influence of three-dimensional roughness of rock fracture on seepage characteristics based on the digital image technology. Arab J Geosci 11:778
Zimmerman RW, Bodvarsson GS (1996) Hydraulic conductivity of rock fractures. Transp Porous Media 23(1):1–30
Zimmerman RW, AI Yaarubi A, Pain CC, Grattoni CA (2004) Nonlinear regimes of fluid flow in rock fractures. Int J Rock Mech Mining Sci 41(3):163–169